Gimeno, J.; Venegas, O.; Urbano, J. (2022). Stress Concentration Factor in vessels with circular crosshole: Continuous parameters analysis. International Journal of Pressure Vessels and Piping. 199:1-10. https://doi.org/10.1016/j.ijpvp.2022.104775

Stress Concentration Factor in Vessels with Circular Crosshole: Continuous Parameters Analysis

Jaime Gimeno[a], Oscar Venegas[b,*], Javier Urbano[b]

[a] *Universitat Politècnica de València, Valencia, Spain*
[b] *Colombian School of Engineering Julio Garavito, Bogotá, Colombia*

*Corresponding author: oscar.enegas@escuelaing.edu.co (Oscar Venegas)

Abstract

In this paper, a parametric study of the Stress Concentration Factor (SCF) has been carried out in cylindrical pressure vessels with circular holes. A three-dimensional finite element analysis has been carried out performing a variation of dimensionless parameters (thickness ratio, size ratio and aspect ratio) exploring a wider range than other investigations, using dimensionless parameters (thickness ratio, size ratio and aspect ratio) with a wider study range compared to other investigations. It is observed that the maximum value of the SCF increases as the hole size ratio and the aspect ratio increase, although the location of the maximum SCF is located from the internal area of the vessel to the external part depending on the geometric configuration, defining thus three differentiated zones. Additionally, in the final part of the document, a fit model is defined to determine the value of the maximum SCF for different continuous values of the defined dimensionless parameters. This model allows to quickly calculate or locate from a contour map the maximum value of SCF for a specific geometry of pressure vessel.

Keywords: stress concentration factor, thick pressure vessels, crossholes, high-pressure vessels, finite element method.

1. Introduction

Pressurized vessels (tanks and pressurized fluid pipelines) have various applications both in industrial processes and research, and holes are commonly found in their walls to connect with other elements or accessories related to the process to be developed, to measure some variable or simply as sight window [13,16,18,22]. The presence of these holes in the pressure vessels, acts as a concentrator of stresses, increasing significantly the local stress than those present at normal section of the vessel, without any concentrator. The stress concentration depends mainly on the geometric characteristics of the vessel, the hole, its position, alignment and inclination [19].

Cite as:
Gimeno, J., Venegas, O., Urbano, J., "Stress Concentration Factor in vessels with circular crosshole: Continuous parameters analysis", International Journal of Pressure Vessels and Piping (2022), Vol. 199, 104775, https://doi.org/10.1016/j.ijpvp.2022.104775

An important indicator is the Stress Concentration Factor (SCF), which relates the maximum stress near of hole in the vessel, with the maximum stress of the same container without hole. This indicator is often used in the design of pressurized cylindrical vessels to preliminarily estimate the stresses to which the vessel is subjected and thus determine different additional variables such as size, thickness, geometry and indirectly make a budget of the project.

The aim of this paper is to study the behavior of SCF in cylindrical pressure vessels with circular holes through its wall, with the thickness ratio, the aspect ratio or slenderness and the size ratio of the hole with respect to the internal diameter of the cylinder as variables. To get a global understanding of SCF behavior, the parametric variation range of the considered variables is wider than what explored in other studies [2,14,15,17,23], and the location of maximum stress and SCF maximum values due the hole have been determined using a Finite Element Analysis (FEA) software.

This document is structured in six sections. Section 2 shows the state of the art related to behavior of SCF pressure vessels with holes. In section 3, the parameters and operating conditions established for the simulations are disclosed, as well as the identification of the points of interest where the maximum SCF is presented. Subsequently, section 4 presents the results and its discussion, including SCF value and location analysis respect to variations of geometric parameters and the contrast with the data found by other authors.

In section 5, a correlation from the continuous analysis of the three geometric relationships previously established in the study (thickness ratio, aspect ratio and hole size ratio) is proposed, in order to mathematically predict the value of the SCF for any geometry that can be used in a cylindrical pressure vessel. Finally, section 6 presents the main conclusions of the study and possible future work.

2. Theoretical background

Geometric variables related to this type of concentrators are mainly derived from the geometry of the vessel and the holes they have. According to Figure 1, the following geometric variables are defined in a closed end cylindrical vessel with a crosshole: main cylinder length (L), outer radius of the cylinder (R_e), inner radius of the cylinder (R_i) and hole radius (R_a).

The relationships between these geometric variables define dimensionless parameters that enable to compare to related investigations [4,11,20]. These dimensionless relationships are defined as: thickness ratio (R_e / R_i) obtained from relating the external and internal radius of the cylinder, aspect ratio or slenderness calculated from the ratio between cylinder length and the outer diameter ($L / 2R_e$), and the size ratio of the hole derived from the ratio between the radius of the hole and the inner radius (R_a / R_i).

Other authors have used similar parameters, with some variations in their definitions and values [11,19]. Specifically, aspect ratio or slenderness values are defined based on specific investigation objectives, and their definition is different and in some cases are not clearly indicated. Makulsawatudom et al. [14] and Camilleri et al. [2] used a ratio of $L / 2R_e = 1$; Dixon

et al. [4] used the Decay cylinder length concept, Masu [15] used $L/2R_e \geq 2$; Kharat [9] used a ratio $L/2R_e = 3$; Iwadate et al. [8] used a $L/2R_e$ ratio between 2.7 and 3.2; Raju [23] used a ratio $L/2R_e = 1.2$; and finally Kihiu et al. [12], Adenya [1] and Nihous [19] used a L value of nine times the wall thickness. The ranges of the parameters considered by the cited authors are summarized in Figure 2.

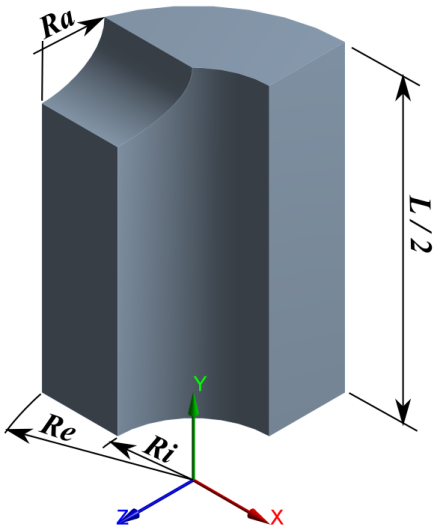

Figure 1: Reference geometry and nomenclature in cylindrical vessels.

In any case, the SCF calculated by several authors retains the concept of relating the maximum stress of the vessel with hole and the maximum stress of the same vessel without hole. The maximum tangential stress on a cylinder without a hole is calculated with equation (1) proposed by Lamé [24], where R_e and R_i, are respectively the external and internal radii of the vessel and p is the internal pressure of the vessel. Lamé equations assume a homogeneous and isotropic material with linear elastic deformations.

$$HoopStress = \sigma_{Hoop} = p\left[\frac{R_e/R_i{}^2+1}{R_e/R_i{}^2-1}\right] \quad (1)$$

In closed ends cylindrical vessels without crosshole, the tangential stress (σ_θ) or Hoop Stress (σ_{Hoop}), are equal to the maximum main stress (σ_{1max}). However, to perform the calculation of the SCF in pressure vessels with crosshole, different relations are used according to the specific aim of the study and there is not consensus among the authors. The maximum stresses and their respective SCF are indicated as: the maximum tangential or hoop stress ($\sigma_{\theta max}$) and $SCF_{\theta max}$ (equation 2), the maximum main stress (σ_{1max}) and SCF_{1max} (equation 3), the maximum shear stress (τ_{max}) and $SCF_{\tau max}$ (equation 4), and the maximum equivalent or maximum von Mises stress (σ_{emax}) and $SCF_{\sigma emax}$ (equation 5), where σ_{ec}, is the value of the equivalent stress of plain cylinder calculated from the Lamé solution [3].

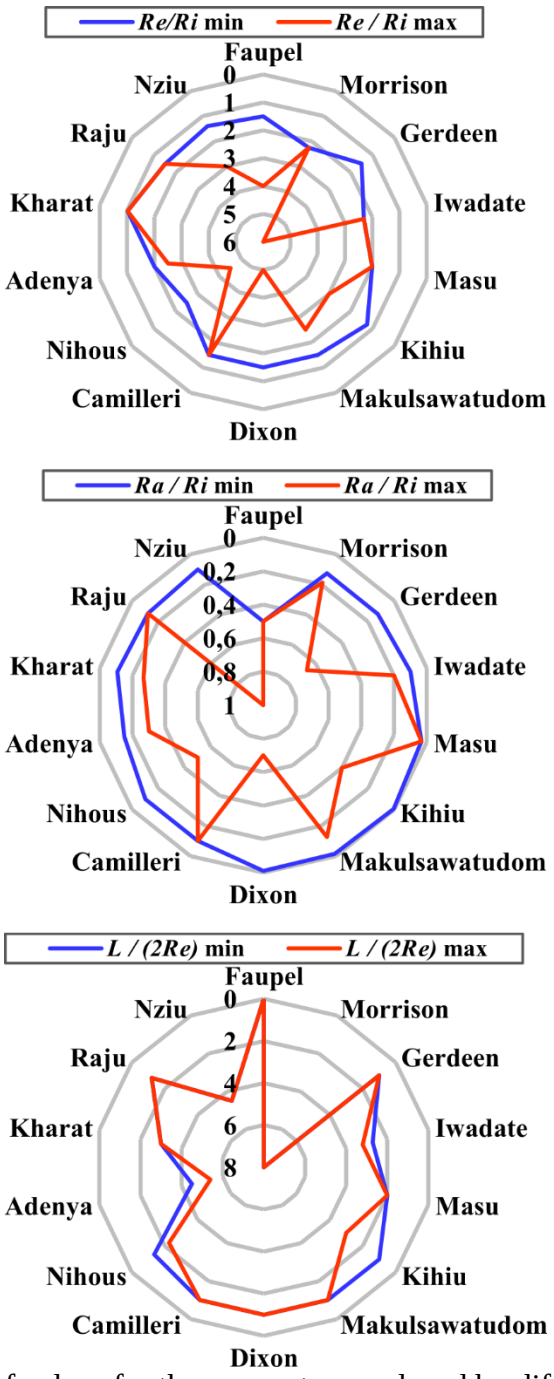

Figure 2: Ranges of values for the parameters analyzed by different authors.

$$SCF_{\theta max} = \frac{\sigma_{\theta max}}{\sigma_{Hoop}} \tag{2}$$

$$SCF_{1max} = \frac{\sigma_{1max}}{\sigma_{Hoop}} \tag{3}$$

$$SCF_{\tau max} = \frac{2\tau_{max}}{\sigma_{Hoop}} \tag{4}$$

$$SCF_{\sigma emax} = \frac{\sigma_{emax}}{\sigma_{ec}} \tag{5}$$

Table 1 presents a summary of types of SCF estimated by each author using equations 2-5 and the methodology employed. The SCF values found by each author vary depending on the relationships established, and the way in which the study was conducted, either analytically, by finite element models or experimental test.

Autor	$\sigma_{\theta max}$	σ_{1max}	τ_{max}	σ_{emax}	***FEM***
Faupel [6] [a]	X				
Morrison [17] [a]	X		X		X
Gerdeen [7] [b]	X				
Iwadate [8] [a]	X				
Masu [15]		X			X
Kihiu [12]	X				X
Comlekci [3]		X		X	X
Dixon [5]		X	X		X
Camilleri [2]	X				X
Nihous [19]		X			X
Adenya [1]	X				X
Kharat [9] [a]	X				
Raju [23]	X			X	X
Nziu [20]	X				X

Table 1: Types of calculated stress and related methodology.
[a] Experimental method, [b] Analytic method

The following sections present a global study, using wider ranges of geometric relations, allows comparison with other results found in the literature. This approach, also enable to learn more about the trend in location and value of the maximum SCF in cylindrical vessels with holes.

3. Simulation setup and validation

In this study, it is considered a thick-walled cylinder with closed ends and a crosshole whose geometric variables, R_a, R_e, R_i and L, as shown in Figure 1, related to each other to obtain dimensionless parameters that can be subsequently compared to the results obtained by other authors. For the cylinder with crosshole centered on both, length and diameter, 1008 models were considered taking different values of geometric relations, R_e / R_i, $L / 2R_e$ and R_a / R_i as shown in Table 2. A fixed value of R_i was defined for all models, 100mm, similar to the study conducted by Comlekci et al. [3]. Values lower than $R_e / R_i = 1.125$ were not considered since usually considered to correspond to the thin sheet theory which is beyond the scopes of this study. According to the range given in Table 2, the L values were between 84mm and 1600mm; R_e between 112mm and 400mm and R_a between 1.25mm and 98.75mm; considering that in the range of R_a / R_i between 0.9 and 0.9875 for values of $L / 2R_e$ equal to 0.625, 0.75 and 0.875 are geometrically incompatible.

Parameter	*Values*
R_e / R_i	1.125, 1.25, 1.5, 1.75, 2, 2.25, 2.5, 3, 4
R_a / R_i	0.0125, 0.025, 0.05, 0.075, 0.1, 0.2, 0.3, 0.4, 0.5, 0.6, 0.7, 0.8, 0.9, 0.95, 0.975, 0.9875
$L / 2R_e$	0.625, 0.75, 0.875, 1, 1.5, 2, 3, 4

Table 2: Established values for the simulations.

To study the effect of geometry on generated stresses for a cylindrical pressure vessel, the simulation was conducted using ANSYS Workbench, applying parametric functionality to vary the dimensional values of the cylinder and holes to get the parameters values predefined and specific results (maximum principal stress and its 3D position). For all simulations, the modeling of 1/8 of a symmetrical cylinder was performed, with respect to three planes of symmetry (Figure 3). First plane (face E) is perpendicular to the base F that passes through the center of the cylinder and the hole, the second plane (face D) perpendicular to face E and base F and passes through the center of the cylinder and the third plane (face C) parallel to base F and passes through the center of the hole. Figure 3 (left side), shown an example of the geometry used for simulations.

An unstructured mesh using three dimensional tetrahedral solid elements, *10−node* isoparametric (Solid187 elements) was used in order to adapt mesh to huge number of models. Because the variation in stress values occurs mainly around the edges and corners near the hole, and according to the FEA results of Comlekci [3] and Nihous [19], a local refinement was included for the mesh. Figure 3 (right side) shown the refinement detail. This refinement, similar to Nihous [19], leads sizing of the elements close to the selected edges achieving a balance between the processing time and the reliability of the data obtained in the area of interest, getting a precise identification of the position of the maximum principal stress in zones nearest or along the edges of the hole. Due to the dimensional difference of the models presented in Table 2, especially the length, reference mesh sizes were used, carrying out the respective mesh convergence for each model; thus obtaining, in general, seed elements from 5mm and adapted according with total volume for each model.

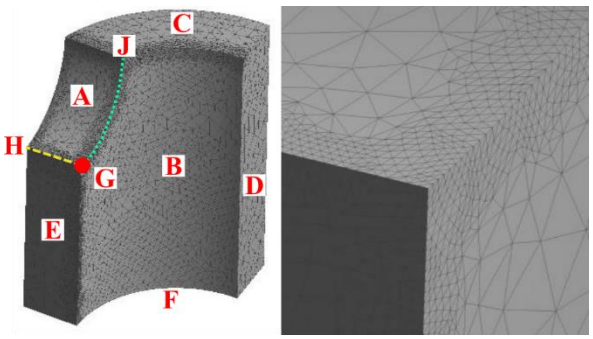

Figure 3: Mesh of 1/8 cylinder. Left-General view, Right-Refinement in areas of interest.

Regarding the boundary conditions, a vessel with closed ends was assumed, then, base F was studied as completely rigid, while the faces D and E were considered deformable in the radial and longitudinal directions. In addition, a distributed load was applied to face C according to the load applied by the rigid closed ends, taking into account 1/4 of this load and the geometry for

each simulation. The internal pressure of the cylinder for all simulated models was imposed at 17.5Mpa and this value was applied both to the internal surface of the cylinder (B) and to the surface of the hole (A). To analyze each model, a carbon steel material with a modulus of elasticity of 200Gpa, a Poisson's ratio of 0.3, a yield strength (S_y) of 250Mpa and an ultimate strength (S_u) of 400Mpa was used, applying a linear stress analysis. Table 3 summarizes main issues related to simulation.

Information	***Description***
Software	ANSYS Workbench
Element	3Dsolid 10−node isoparametric, Solid187
Mesh	Unstructured Mesh. Refined in specific Edges
Symmetry	3 planes
Internal Pressure	17.5MPa
Material	Carbon Steel Linear elastic
Analysis Type	Parametric Linear elastic
Geometric variables	R_e / R_i, R_a / R_i and $L / 2R_e$
Output	Max Principal Stress and its 3D Location
Simulated models	1008

Table 3: Simulation conditions.

In order to validate the parametrization of the mesh, simulations of vessels without hole ($R_a / R_i = 0$) are initially performed for all ranges of R_e / R_i and $L / 2R_e$ shown in Table 2 and these results are compared with equation 1 proposed by Lamé. In Figure 4, it is observed that the principal stress values for different thickness and aspect ratios are properly adjusted to the Lamé equation, finding a maximum average deviation of 8.5% for the thickness ratios R_e / R_i smaller and tending to decrease to one third at higher values of R_e / R_i, showing that the mesh parameterization used in the simulations is consistent with the Lamé equation. In general, it is observed that for aspect ratios $L / 2R_e$ less than unity and for values of R_e / R_i close to 1, the deviations of the simulation with respect to the calculation with equation 1 increase. A final post process was performed to estimate the SCF_{1max} (equation 3), from σ_{1max} obtained from simulations and σ_{Hoop} calculated from Lamé equation.

4. Results and discussion

In this section, the results obtained from the simulations are shown taking into account the different possible combinations of Table 2, where an elastic linear analysis was carried out, finding that in most of the cases analyzed (approximately 60%) the maximum SCF is located in the G corner of the hole (see Figure 3 left side), which in agreement with various studies that define corner G as the most critical [14,20]. However, Nziu [20] highlights that for certain configurations of R_a / R_i and R_e / R_i, the maximum stress was not found in the corner G of the hole but on the edge adjacent to the cylinder (edge G-J in the Figure 3 left side).

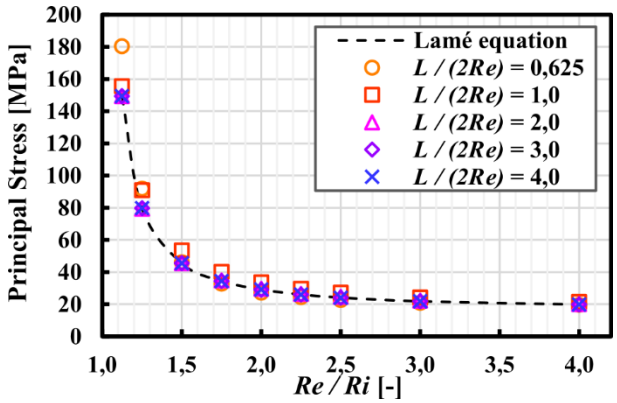

Figure 4: Validation of mesh parameterization with Lamé's equation for cylinders without holes.

From the results obtained from the present study, it is observed that in thick-walled cylinders with very small holes, the location of the point of maximum stress moves from the corner G to the exterior of the cylinder (edge G-H in Figure 3 left side), such as it is observed in Figure 5 for a 75mm thick wall thickness with a maximum stress located 1mm from the corner G on the edge G-H. Figure 6 shows a cylinder with the same values of R_a / R_i and $L / 2R_e$ of the previous case but with a thicker wall, 200mm, showing that the behavior is similar to that shown previously, moving along the edge G-H outwards.

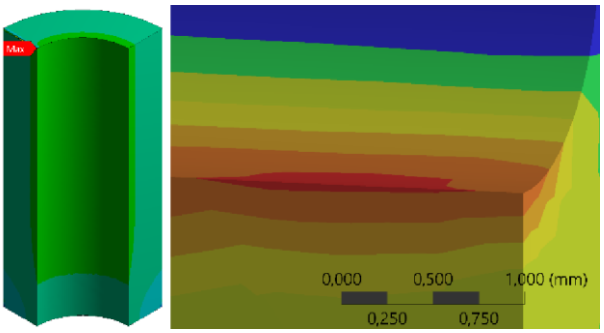

Figure 5: Point of maximum stress for $R_a / R_i = 0.0125$; $R_e / R_i = 1.75$ and $L / 2R_e = 3$. Left-General View and Right-Detail of the position of the maximum main stress point.

On the other hand, when reviewing values of $R_e / R_i = 1.125$ and $L / 2R_e = 1.5$ for different values of R_a / R_i; the displacement of the maximum point SCF is notable. In Figure 7a, it is observed that for values of R_a / R_i close to 0.5 the point of maximum principal stress is located slightly away from the corner G on the edge G-J and as the ratio R_a / R_i increases, the maximum SCF moves on the same edge (G-J) moving further away from the corner G (Figure 7b), even reaching values close to $R_a / 2$ (Figure 7c). In other more critical cases, as R_a / R_i approaches 1, the point of maximum stress after moving away from G on edge G-J, also moves outwards, thus finding the maximum SCF covering part of face A as seen in Figure 7d and Figure 7e. The above is an extreme case, close to the theory of a thin sheet for vessels (cylinder wall thickness is less than 10% of the cylinder radius [24]), which makes it difficult to propose an analytical theory, due to the change in position point of maximum stress. Finally, for values of $L / 2R_e$ less

than unity, the behavior is similar to that shown in Figure 7d and Figure 7e; i.e , the maximum SCF is presented on face A.

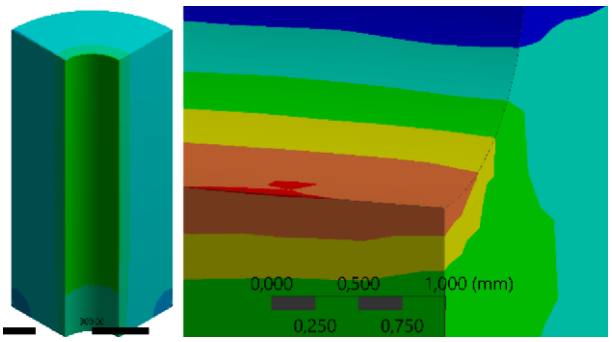

Figure 6: Point of maximum stress for $R_a / R_i = 0.0125$; $R_e / R_i = 3$ and $L / 2R_e = 3$. Left-General View and Right-Detail of the position of the maximum main stress point.

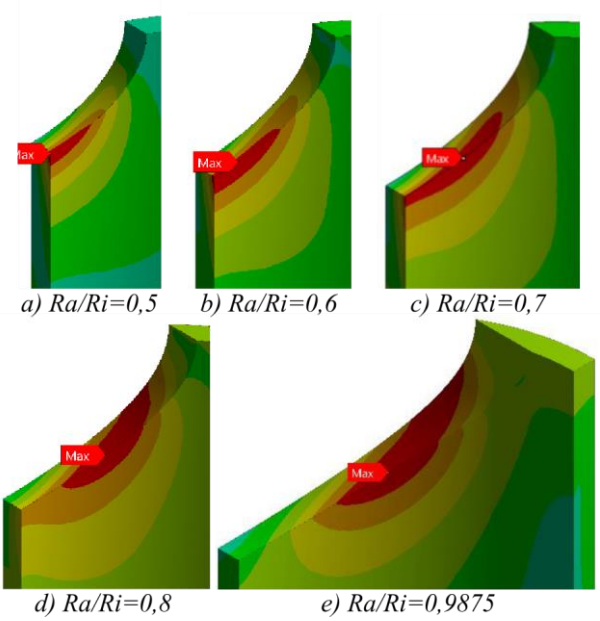

a) Ra/Ri=0,5 *b) Ra/Ri=0,6* *c) Ra/Ri=0,7*

d) Ra/Ri=0,8 *e) Ra/Ri=0,9875*

Figure 7: Point of maximum stress for $R_e / R_i = 1.125$ and $L / 2R_e = 1.5$.

Figure 8 represents the location of the maximum SCF presenting the percentage of the radius of the hole R_a on the abscissa (X axis), showing how far the maximum SCF is from corner G along edge G-J, and on the ordinate (Y axis) the percentage of wall thickness, showing how far the maximum SCF is from the corner G by the normalized edge G-H with respect to the thickness of the cylinder. Figure 8 shows that most of the cases are in the area near the corner G, especially on the edge G-J, edge G-H and on the surface A. The other points are seen on the surface A and in some of the simulated cases, the point of maximum SCF extends to outer cylinder wall (100% wall thickness).

In order to deepen and link the location of the points in Figure 8 with the thickness ratio (R_e / R_i) and the hole size ratio (R_a / R_i) for all aspect ratio ranges ($L / 2R_e$) studied, in Figure 9 different zones are shown depending on these relationships.

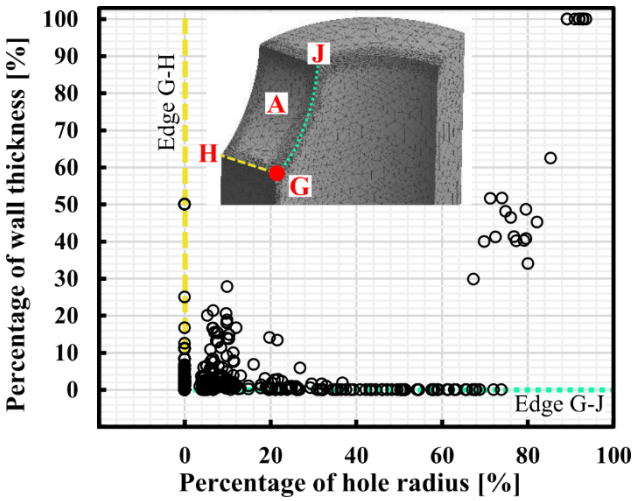

Figure 8: Location of the maximum SCF for all the values studied.

It is possible to see that for all the cases of $R_a / R_i = 0.3$, independent of the other variables, the point of maximum SCF is located in the corner G, which coincides with the studies of Nziu [21]. Thus, the Figure 9 is divided into three zones, depending on the possible combinations with the other geometric relationships throughout its range. A first zone named Z1 for combinations with values of $R_a / R_i > 0.3$; a second zone called Z2 for combinations with $R_a / R_i = 0.3$, and a third zone called Z3 for combinations with $R_a / R_i < 0.3$.

Zone Z1, is delimited by the blue dotted line, corresponding to values of $R_a / R_i > 0.3$ and where the points of maximum SCF move moving away from point G on edge G-J as R_a / R_i increases until it reaches a value close to 0.5, where the distance is approximately 70% of the hole radius, and then moving away towards the center of surface A for values of $R_a / R_i > 0.5$ reaching in some cases up to the outer wall of the cylinder. The Z3 zone delimited by the solid red line corresponds to values of $R_a / R_i < 0.3$, where the maximum point SCF is not located beyond 40% of the hole radius and all the values of this zone come off the surface internal up to a maximum of 50% of the wall thickness. As the values of R_a / R_i approach zero, the values have more dispersion in the delimited zone; which may be an effect of the size of the hole in the model and it is consistent with most of the Nziu data [21].

The zones previously described show the limit zones of the values of R_a / R_i. It is also possible to see that for the same value of R_a / R_i, the limits for the values of R_e / R_i close to 1.25 tend to be further away from the internal surface of the cylinder, while those values closer to 3.0 are closer to both the inner surface and the corner G. Figure 10 clearly shows this last variation for R_e / R_i in the area near the corner G. The variations of $L / 2R_e$ distribute the data in the areas delimited by the other two variables, making the locations move towards or away from the G corner.

The detail of the position in zones close to the corner G (Figure 10), can be very useful for designers of this type of vessels, since it allows easy positioning the maximum SCF or at least know the tendency that these may present in failure analysis investigations with similar

geometric relationships.

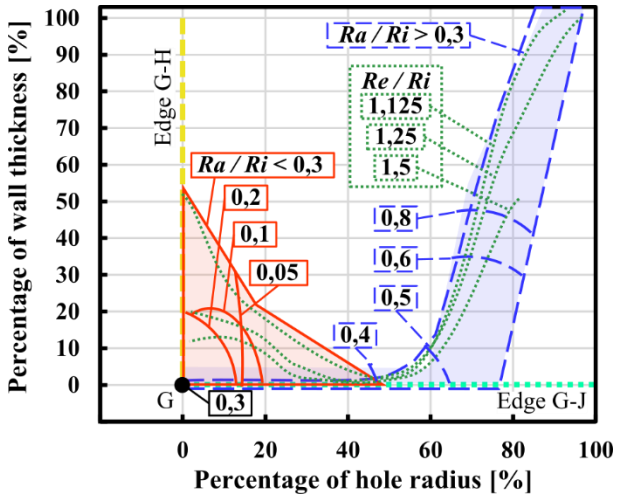

Figure 9: Maximum SCF location zones.

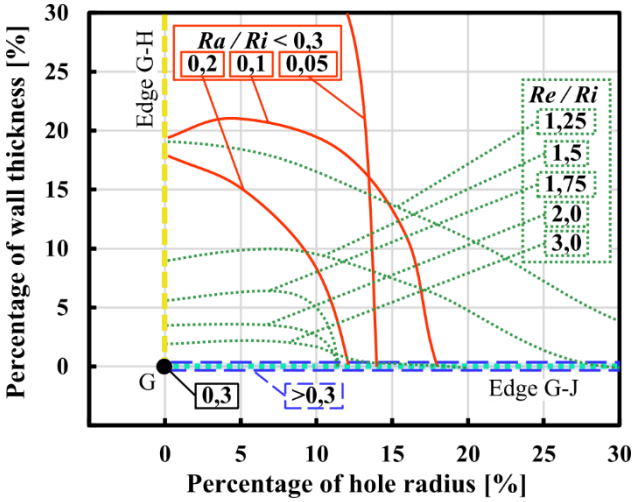

Figure 10: Detail of the location zones of the maximum SCF.

Figure 11 shows the location of these maximum points as a function of the combinations of R_a / R_i, R_e / R_i and $L / 2R_e$ and the zones described above, which are delimited by envelopes with iso-values of $L / 2R_e$. In Figure 11 the values of $L / 2R_e = 2$ are shown, since it is a value widely used in this type of study and the directions to where these enveloping limits move are indicated with arrows.

Analyzing Figure 11, when using combinations of values of $R_a / R_i > 0.3$ and $R_e / R_i > 1.75$ the position will always be in the corner G (zone Z2). For combinations of values of $R_a / R_i > 0.3$ and $R_e / R_i < 1.75$ and depending on the envelopes $L / 2R_e$, the maximum point SCF will be located in zone Z2 or in the zone Z1. For combinations of values of $R_a / R_i < 0.3$ and $R_e / R_i > 1.5$, it depends on the value of $L / 2R_e$; thus, for values of $L / 2R_e$ close to the lower limit of the study, 0.75, the point of maximum SCF is in the corner G; as the values of the envelopes $L / 2R_e$ increase, the

probability that the maximum point SCF is in zone Z2 increases, too.

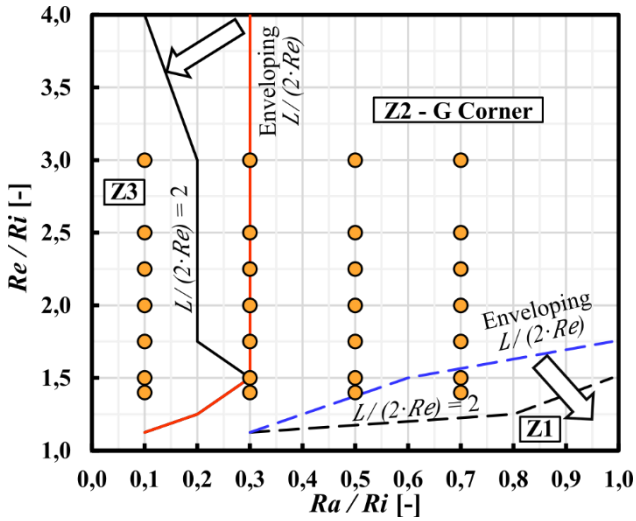

Figure 11: Location of maximum point of SCF and comparison with data from Nziu and Masu [18] (circles).

The results shown in zone Z3 of the present study coincide with the results of Masu [15], Makulsawatudom [14], Kihiu [10] and Adenya [1]. Also, the results of the present study are consistent with the data of Nziu y Masu [21] (shown as circles in Figure 11), which provide more information on the positions of the maximum SCF.

Figure 12 shows a comparison between some values of R_e / R_i for $L / 2R_e = 2$ with the data of various authors who evaluated cylinders with through holes such as Masu [15], Dixon [4], Nihous [19] and Nziu [20], finding average percentage deviations lower than 6% and with a standard deviation of 0.084.

Finally, in Figure 13, the maximum SCF data for all ranges of the dimensionless parameters studied in this document are exposed, showing that for each value of $L / 2R_e$ the SCF increases as parameter R_e / R_i gets smaller for values of R_a / R_i between 0.2 and 0.4; for values of R_a / R_i less than 0.1 the SCF increases as the parameter R_e / R_i is larger and lastly, values of R_a / R_i greater than 0.4 do not follow the same trend for small values of R_e / R_i (1.125, 1.25 and 1.5). 9.1 was the highest SCF value found (for $R_e / R_i = 1.25$; $L / 2R_e = 4$; $R_a / R_i = 0.9875$) and the lowest value was 2.4 (for $R_e / R_i = 1.25$; $L / 2R_e = 0.0625$; $R_a / R_i = 0.6$). For all values of R_e / R_i with values of $L / 2R_e > 0.75$, and R_a / R_i nearest to 0.1, the SCF values are between 2.8 an d 3.2 showing a commune zone of inflection, that are also shown by other authors and suggest a relative low sensibility to the R_e / R_i, and $L / 2R_e$ parameters for $R_a / R_i = 0.1$ values.

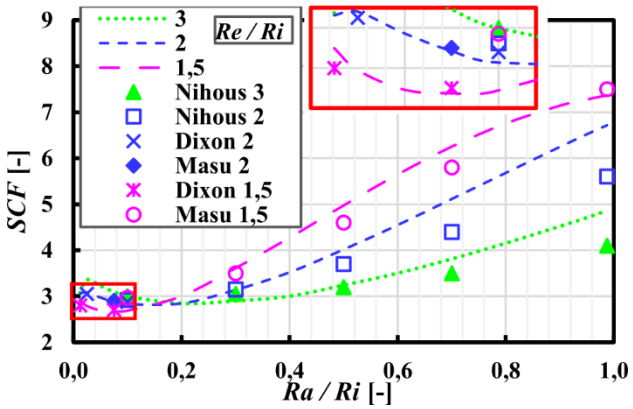

Figure 12: Comparison of SCF from simulations (lines) with other authors for $L/\ 2R_e\ = 2$ and different values of $R_e\ /\ R_i$.

5. Fit model using dimensionless parameters

Once all the results of the simulation have been obtained, Figure 13 shows the effect of the geometric relationships on the SCF. It is of great interest for the design of pressure vessels with large holes, to have an equation that allows to easily finding the value of SCF for a specific geometric configuration, based on the geometric relationships discussed in the previous sections. In this way, in order to obtain an adequate fit model, the authors initially analyze the sensitivity of SCF to $R_a\ /\ R_i$ while keeping $R_e\ /\ R_i$ and $L/\ 2R_e$ fixed. Subsequently, only parameter $L/\ 2R_e$ is kept fixed and it is observed how SCF varies as a function of $R_e\ /\ R_i$. According to these variations, the authors propose equation 6, which does not have a physical or theoretical meaning of the SCF, but of the effect of the geometric relationships ($R_a\ /\ R_i$ and $R_e\ /\ R_i$) in SCF obtained from the simulations. The variables included in the model are limited to $R_a\ /\ R_i$ and $R_e\ /\ R_i$ for different values of $L/\ 2R_e$, to limit the complexity and length of the model.

$$SCF = \zeta - \lambda \cdot e^{-\tau\ R_a/R_i} \cdot cos\left[\omega\ R_a\ /\ R_i\ + \phi\right] \tag{6}$$

where;

$$\zeta = A + B \cdot sin\left[C \cdot\ R_e\ /\ R_i\ + D\right]$$

$$\lambda = E * cos\left[G \cdot\ R_e\ /\ R_i\ + H\right] + I$$

$$\tau = J + K \cdot\ R_e\ /\ R_i$$

$$\omega = L' \cdot e^{M\ R_e/R_i} \cdot cos\left[N \cdot\ R_e\ /\ R_i\ + O\right] + P$$

$$\phi = Q \cdot e^{R' \cdot \Psi} \cdot cos\left[S \cdot \Psi + T\right] + U$$

$$\Psi = R_e\ /\ R_i - 0.65$$

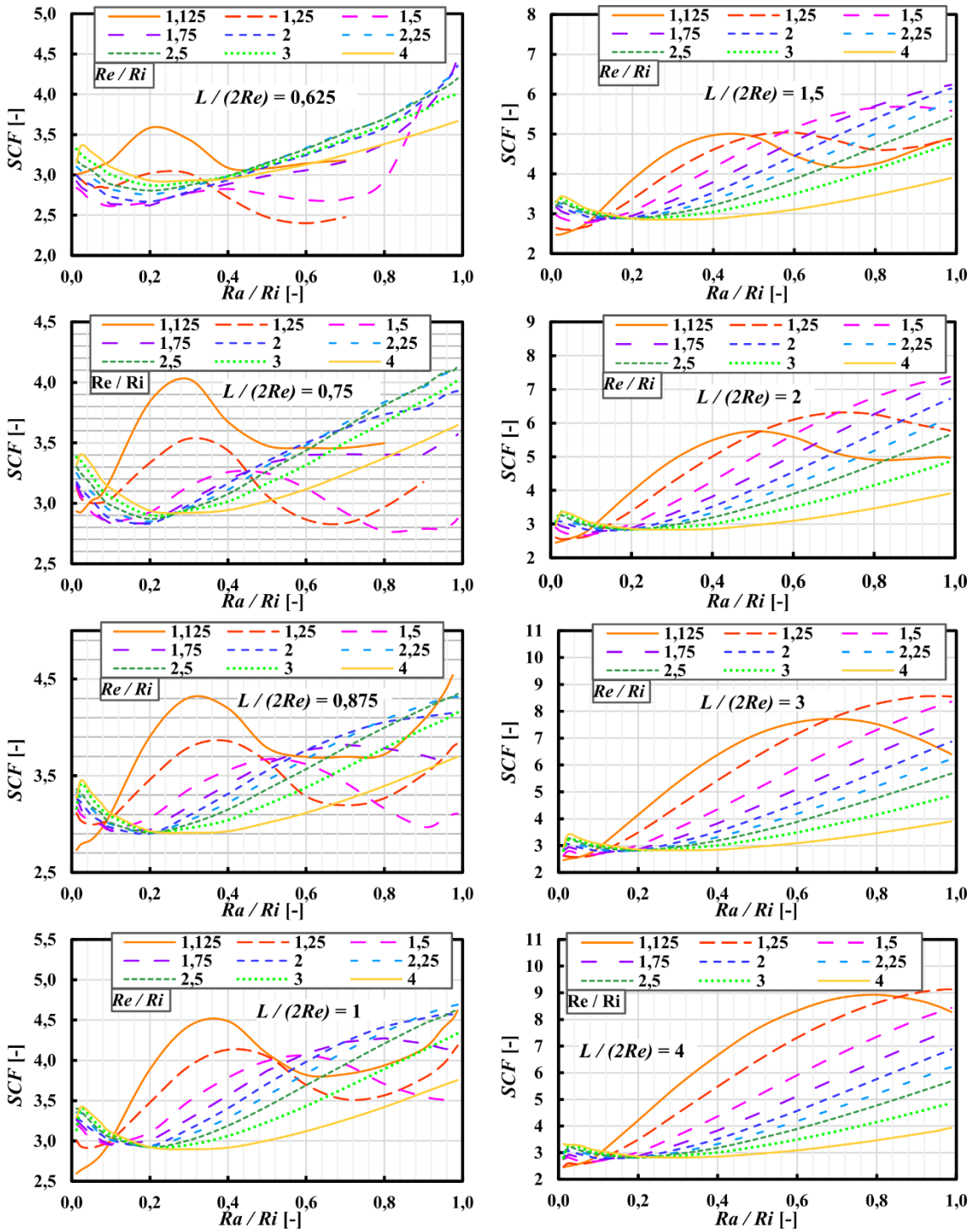

Figure 13: Evolution of SCF for different values of R_e / R_i, R_a / R_i, and $L / 2R_e$.

To this aim, the authors use the Statgraphics software, which allows statistical determination of the values of each of the constants (A to U) of equation 6, taking into account the evolution shown in Figure 13. In this way, the global fit model presented in equation 6, predicts the stress concentrator factor (SCF) as a function of the size ratio (R_a / R_i), the thickness ratio (R_e / R_i) and applies to different aspect ratio ($L / 2R_e$) by varying the constants from A to U (Table 4, Table 5

and Table 6).

As an example, for $L/2R_e = 2$, Table 4 shows the estimated values for each constant (A to U) through the statistical study using the Marquardt estimation method (Statgraphics software), with a correlation coefficient R^2 of 99.08%, showing a good fit of the proposed model to the simulation data obtained. Table 4 shows the asymptotic error and the intervals (lower and upper) for a 95% confidence interval.

	Estimate	***Error***	***Lower***	***Upper***
A	5.87243	0.0980817	5.67842	6.06645
B	2.35371	0.0561608	2.24262	2.4648
C	-107.97	1.23176	-110.407	-105.534
D	320.078	2.60091	314.933	325.222
E	-5.67637	0.139752	-5.95282	-5.39993
G	-116.331	0.660023	-117.636	-115.025
H	67.718	2.50167	62.7695	72.6666
I	5.3465	0.209388	4.93231	5.76069
J	3.61627	0.114802	3.38917	3.84336
K	-0.85885	0.0452558	-0.948371	-0.76933
L'	1976.53	278.557	1425.51	2527.55
M	-0.968788	0.0625958	-1.09261	-0.844967
N	-42.6847	2.27992	-47.1946	-38.1748
O	-388.765	3.5646	-395.816	-381.713
P	209.342	9.00266	191.534	227.15
Q	328.936	77.8571	174.926	482.945
R'	-2.13934	0.283113	-2.69937	-1.57931
S	34.0433	7.14803	19.9037	48.1828
T	-659.491	6.50134	-672.352	-646.631
U	-58.1806	1.58785	-61.3216	-55.0397

Table 4: Statistically estimated constants for $L/2R_e = 2$.

Figure 14 shows the evolution of SCF obtained from the model (equation 6) for an $L/2R_e = 2$ for different values of R_a/R_i and R_e/R_i. When comparing Figure 14 (model) with Figure 13 (for the same value of $L/2R_e = 2$), the good fit obtained statistically is evidenced, showing negligible differences when R_a/R_i approaches zero.

Similarly, the fit model (equation 6) is applied for different values of $L/2R_e$ and for each of these the constants and the correlation coefficient (R^2) are obtained again as shown in Table 5 and Table 6. The variable $L/2R_e$ has not been introduced in the correlation (equation 6) in order not to be excessively complex.

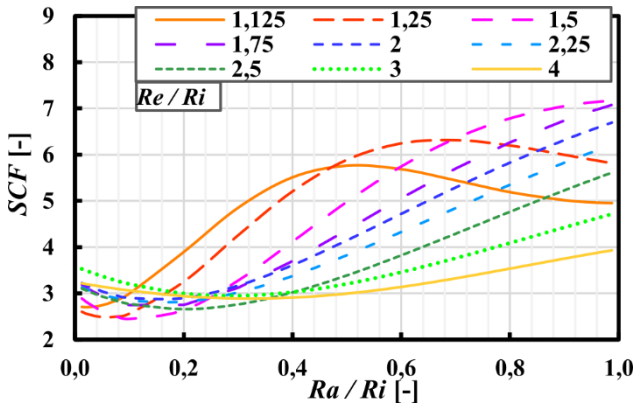

Figure 14: SCF obtained from the model for $L/\ 2R_e = 2$.

	$L/\ 2R_e$			
	0.625	***0.750***	***0.875***	***1.000***
A	5.17719	4.58489	4.82469	4.99127
B	2.35575	1.51165	1.39513	1.22057
C	-119.922	-114.529	-98.0588	-102.245
D	433.053	441.797	423.765	423.419
E	-3.59702	-2.35017	-2.01924	-2.01616
G	-123.512	-119.201	-104.127	-111.739
H	164.343	174.543	160.867	164.606
I	3.58965	2.44007	2.52638	3.04155
J	2.04636	3.18506	2.41475	3.35661
K	-0.44879	-0.794853	-0.519778	-0.774697
L'	4914.59	3773.13	2848.51	3204.92
M	-0.57629	-0.398451	-0.308604	-0.324903
N	-20.1416	-18.9695	-17.92	-16.1582
O	-426.597	-431.345	-434.216	-436.537
P	583.565	756.521	763.487	764.764
Q	3686.35	307.061	242.66	270.22
R'	-3.73822	-1.22322	-1.06648	-0.910646
S	36.1436	38.3746	33.9955	30.1892
T	-656.486	-657.797	-648.241	-643.339
U	-52.1502	-37.4654	-35.5196	-28.9093
R^2	***86.6%***	***89.1%***	***92.9%***	***96.8%***

Table 5: Statistically estimated constants for $L/\ 2R_e < 1$.

The tabulated values in Table 5 and Table 6, are useful in future studies to obtain an exact value of the SCF as a function of the dimensionless parameters R_e/R_i, R_a/R_i and $L/\ 2R_e$. Figure 15 shows a contour map that allows to quickly locate and know the value of SCF for any value of R_e/R_i, R_a/R_i and $L/\ 2R_e$ within the ranges established in this study (Table 2). In this way, values of $R_e/R_i \leq 2$ the SCF increases as $L/\ 2R_e$ and R_a/R_i increase and for values of $R_e/R_i > 2$ the SCF is no longer dependent on the aspect ratio $L/\ 2R_e$. In Figure 15, the small

dark areas (for R_e / R_i equals 1.125, 1.25 and 1.5), represent geometrically incompatible zones and therefore these combinations were not taken into account during the study.

Finally, comparing the simulation data (Figure 13) with the fit model data (Figure 15), a clear correspondence of the SCF values is observed, although the contour map allows us to observe the continuous behavior of the SCF when varying the dimensionless parameters R_a / R_i and $L / 2R_e$ for each value of R_e / R_i. Thus, it is concluded that the SCF increases gradually as the cylinder aspect ratio increases and the hole size increases, for all values of R_e / R_i.

	$L / 2R_e$			
	1.5	***2.0***	***3.0***	***4.0***
A	5.07909	5.87243	5.89189	5.88183
B	1.53149	2.35371	2.20899	2.16963
C	-86.778	-107.97	-94.9887	-74.6168
D	300.428	320.078	268.044	210.921
E	-2.98539	-5.67637	-4.4904	-4.00222
G	-109.54	-116.331	-108.754	-96.8276
H	73.0618	67.718	42.4599	12.6292
I	4.00825	5.3465	5.26064	5.09826
J	4.29287	3.61627	2.1793	1.86163
K	-1.09777	-0.85885	-0.21861	-0.0734957
L'	2191.99	1976.53	618.216	68.1164
M	-0.506532	-0.968788	-1.10092	-0.200859
N	-17.6558	-42.6847	-94.2791	-110.085
O	-432.097	-388.765	-293.17	-256.044
P	374.406	209.342	136.559	135.763
Q	208.425	328.936	278.119	1026.96
R'	-1.85469	-2.13934	-3.19082	-4.15783
S	67.3123	34.0433	-0.405139	18.8221
T	-686.665	-659.491	-667.505	-664.201
U	-54.4126	-58.1806	-62.6983	-61.5961
R^2	***98.6%***	***99.1%***	***99.0%***	***99.2%***

Table 6: Statistically estimated constants for $L / 2R_e > 1$.

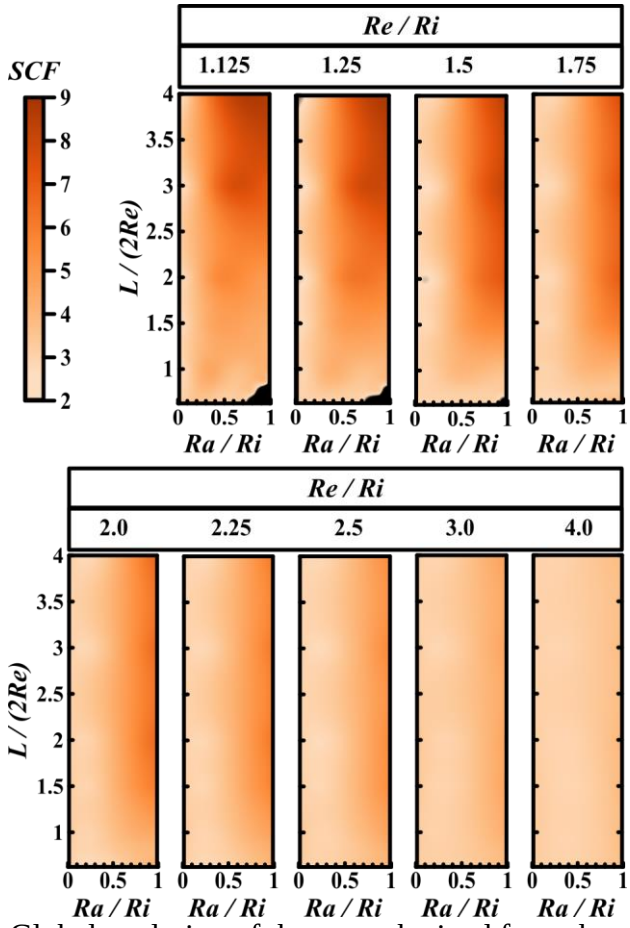

Figure 15: Global evolution of the SCF obtained from the model.

6. Conclusions

In this document, a three-dimensional finite element study was carried out to identify the maximum SCF and its location in pressure vessels with circular crossholes. This study was carried out using a wider range of geometric relationships used by other authors; this aspect enabled not only to compare the results of the present study with the particular results obtained by other authors but also to identify the behavior of the maximum SCF and its location in a wider range of geometric configurations (R_e / R_i between 1.125 and 4, R_a / R_i between 0.0125 and 0.9875, and $L / 2R_e$ between 0.625 and 4).

From state of the art review, there is a lack of consistency in the methodology for the estimation of the SCF for a given geometry in pressurized vessel with orifices, no clear consensus among authors, finding at least four different ways to calculate it: $SCF_{\theta max}$, SCF_{1max}, $SCF_{\tau max}$, $SCF_{\sigma emax}$. In this study, initially a parametric validation of the mesh was carried out using the Lamé equation for cylinders without crosshole, finding a maximum average deviation of 8.5% for the smallest R_e / R_i thickness ratios. Subsequently, for the 1008 models of pressure vessel with crosshole, the maximum SCF 1max has been used and its respective location, establishing in this way three specific zones.

From the established zones, it was possible to identify that in most of the cases analyzed (approximately 60%) the maximum SCF is found in the corner G of the hole that corresponds to zone Z2 with values of $R_a / R_i = 0.3$. The other cases analyzed are distributed in zones Z1 and Z3. The Z1 zone corresponds to values of $R_a / R_i > 0.3$ and where the points of maximum SCF move away from point G up to 70% of the radius of the hole (edge G-J) as R_a / R_i increases. From that 70% it tends to move on the surface A for values of $R_a / R_i > 0.5$, reaching even in some cases up to the external wall of the cylinder. Regarding the Z3 zone for values of $R_a / R_i < 0.3$, the points of maximum SCF are located in an almost triangular area defined by the corner G, 40% of the radius of the hole (edge G-J) and 50% of the wall thickness (edge G-H).

In general, the influence of the aspect ratio, $L / 2R_e$, both on the position and on the value of the maximum SCF was determined, finding that values below 2 have a high impact on the value of the maximum SCF, while values above 3 have no influence on said value. Regarding the location, although it depends on the other variables, small values of aspect ratio place the maximum stress point in zone Z2 (corner G) and high values of aspect ratio place the maximum SCF in zones Z1 or Z3, depending on the values of the other parameters.

Once the maximum SCF and its location have been determined, the information given here is useful for the design of cylindrical vessels with holes with different geometric configurations. In fact, from the present study it has been possible to show that always taking the location of the point of maximum stress in the corner G as a unique design criterion is not suitable, since the maximum value of SCF can move away from the corner G depending on the geometric configuration, according to the zones established in this study.

Finally, a fit model has been proposed, which is statistically representative of the data obtained from finite elements and allows determining the SCF as a function of R_a / R_i and R_e / R_i valid for different values of $L / 2R_e$. Thus, the model defined in equation 6 is useful in the design of pressure vessels with hole, since it allows to obtain in a simple and fast way an accurate value of the maximum SCF by varying the dimensionless parameters. In addition, a contour map has been included, which allows to observe the behavior of the SCF continuously by varying R_a / R_i, $L / 2R_e$ and R_e / R_i. Thus, globally for all the values of R_e / R_i, it is observed that the SCF gradually increases as the relationship between slenderness and hole size increases.

Acknowledgements

The researchers appreciate the support of the Colombian School of Engineering Julio Garavito in the development of the project.

References

[1] C.A. Adenya, J.M. Kihiu, Stress concentration factors in thick walled cylinders with elliptical cross-bores, in: 2010: pp. 181–200.

[2] D. Camilleri, D. Mackenzie, R. Hamilton, Shakedown of a thick cylinder with a radial crosshole, Journal of Pressure Vessel Technology. 131 (2008).

[3] T. Comlekci, D. Mackenzie, R. Hamilton, J. Wood, Elastic stress concentration at radial crossholes in pressurized thick cylinders, Journal of Strain Analysis for Engineering Design. 42 (2007) 461–468.
[4] R.D. Dixon, D.T. Peters, J.G.M. Keltjens, Stress concentration factors of cross-bores in thick walled cylinders and blocks, Journal of Pressure Vessel Technology. 126 (2004) 184–187.
[5] R. Dixon, D. Peters, J. Keltjens, Stress concentration factors of cross-bores in thick walled cylinders and square blocks, American Society of Mechanical Engineers, Pressure Vessels and Piping Division (Publication) PVP. 436 (2002).
[6] J.H. Faupel, D.B. Harris, Stress concentration in heavy-walled cylindrical pressure vessels - Effect of elliptic and circular side holes, Industrial & Engineering Chemistry. 49 (1957) 1979–1986.
[7] J.C. Gerdeen, Analysis of stress concentrations in thick cylinders with sideholes and crossholes, Journal of Engineering for Industry. (1972) 815–824.
[8] T. Iwadate, H. Takeda, K. Chiba, J. Watanabe, Safety analysis at a cross-bore corner of high pressure reactors, Journal of High Pressure Institute of Japan. 23 (1985) 245–253.
[9] A.R. Kharat, V. Kulkarni, Analysis of stress concentration at opening in pressure vessel using ANOVA, International Journal of Research in Engineering and Technology. 03 (2014) 261.
[10] J.M. Kihiu, G.O. Rading, S.M. Mutuli, Overstraining of flush plain cross-bored cylinders, Proceedings of the Institution of Mechanical Engineers, Part C: Journal of Mechanical Engineering Science. 218 (2004) 143–153.
[11] J.M. Kihiu, G.O. Rading, S.M. Mutuli, Universal SCFs and optimal chamfering in cross-bored cylinders, International Journal of Pressure Vessels and Piping. 84 (2007) 396–404.
[12] J. Kihiu, G. Rading, S. Mutuli, Geometric constants in plain cross-bored cylinders, Journal of Pressure Vessel Technology - Transactions of The Asme. 125 (2003).
[13] S.K. Koh, Fatigue analysis of autofrettaged pressure vessels with radial holes, International Journal of Fatigue. 22 (2000) 717–726.
[14] P. Makulsawatudom, D. Mackenzie, R. Hamilton, Stress concentration at crossholes in thick cylindrical vessels, The Journal of Strain Analysis for Engineering Design. 39 (2004) 471–481.
[15] L.M. Masu, Cross bore configuration and size effects on the stress distribution in thick-walled cylinders, International Journal of Pressure Vessels and Piping. 72 (1997) 171–176.
[16] L. Mizzi, A. Spaggiari, Stress concentrations in skew pressurized holes: A numerical analysis, International Journal of Pressure Vessels and Piping. 194 (2021) 104510.
[17] J.L.M. Morrison, B. Crossland, J.S.C. Parry, Fatigue strength of cylinders with cross-bores, Journal of Mechanical Engineering Science. 1 (1959) 207–210.
[18] K.B. Mulchandani, D.P. Shukla, Photoelastic investigation of stress intensifications in the interacting nozzle attachment region of pressure vessels, The Journal of Strain Analysis for Engineering Design. 30 (1995) 167–174.
[19] G.C. Nihous, C.K. Kinoshita, S.M. Masutani, Stress concentration factors for oblique holes in pressurized thick-walled cylinders, Journal of Pressure Vessel Technology. 130 (2008).
[20] P.K. Nziu, L.M. Masu, Cross bore size and wall thickness effects on elastic pressurised thick cylinders, International Journal of Mechanical and Materials Engineering. 14 (2019) 4.
[21] P.K. Nziu, L.M. Masu, Cross bore geometry configuration effects on stress concentration in high-pressure vessels: a review, International Journal of Mechanical and Materials Engineering. 14 (2019) 6.

[22] R. Payri, F.J. Salvador, J. Gimeno, O. Venegas, Study of cavitation phenomenon using different fuels in a transparent nozzle by hydraulic characterization and visualization, Experimental Thermal and Fluid Science. 44 (2013) 235–244.
[23] G. Raju, K.H. Babu, N.S. Nagaraju, K.K. Chand, Design and analysis of stress on thick walled cylinder with and with out holes, Int. Journal of Engineering Research and Applications. 5 (2015) 75–83.
[24] S.P. Timoshenko, J.N. Goodier, Theory of elasticity, 2nd ed., McGraw-Hill Book Company, 1951.